ACS APPLIED MATERIALS & INTERFACES

RESEARCH ARTICLE

www.acsami.org

Direct Comparison of Solution- and Vacuum-Processed Small Molecular Organic Light-Emitting Devices with a Mixed Single Layer

Zhaokui Wang,* Yanhui Lou, Shigeki Naka, and Hiroyuki Okada

Graduate School of Science and Technology, University of Toyama, 3190 Gofuku, Toyama, 930-8555, Japan

Supporting Information

ABSTRACT: It will be interesting and valuable information can be achieved if a direct comparison between organic light emitting devices (OLEDs) fabricated by vacuum evaporated method (vac) and solution-based manufacturing processes (sol) was realized. Small molecular OLEDs with a mixed organic layer structure (MOLOLEDs) make it possible for direct comparison between devices with the same materials but fabricated by the two processing methods. This article shows a direct comparison of the luminescence characteristics, charge conduction, and device physics between MOLOLEDs fabricated by vac- and sol-processing techniques. It gives an elementary explain how the organic/metal interfaces influence the charge conduction and device performance.

KEYWORDS: organic light-emitting devices, mixed organic layer, small molecular organic semiconductor, solution- and vacuum-processed device, conduction mechanism

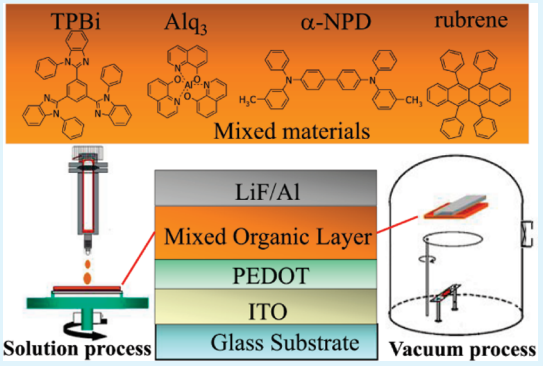

1. INTRODUCTION

Although exciting advances have been made in organic light-emitting devices (OLEDs) since the earlier breakthrough by Tang, VanSlyke, and Chen,[1,2] efficiency, lifetime, and fabrication cost are still challenging issues for commercial requirements in display and lighting applications up to date. A limitation commonly imposed by organic material is that electrons show lower carrier mobility than holes.[3,4] In addition, an energy barrier height between a metal work function and lowest unoccupied molecular orbital (LUMO) or highest occupied molecular orbital (HOMO) of the organic material inhibits carrier injection from an electrode to organic material. Therefore, the device performance is restricted and is not sufficient for practical applications presently. Fortunately, OLED performance is improved by using a multilayer structure with separate electron and hole transporting layers since improved carrier injection and transport.[5] Moreover, recombination zone can be fixed at emission layer using a sandwiched emission layer structure between hole and electron transport layers.[6] However, the presence of a heterojunction interface in the multilayer structure limits the device stability due to accumulation of charges and generation of higher electric field at interfaces. Recently, mixed single-layer structure, in which electron-transport material, hole-transport materials, host, and dopant are mixed in one layer, is proposed for improving a device performance by optimizing the mixing ratio and doping concentration.[7−16] Particularly, Aziz et al. demonstrated that it is possible to resolve the device reliability problem by using a mixed hole-transport and electron-transport layer as the emission layer.[13,16]

In general, there are two processing techniques for the fabrication of OLEDs: vacuum deposition (vac) and solution processing (sol). Vacuum deposition allows for simple fabrication of multilayer architectures layer by layer. However, the process control is complicated, and high-vacuum conditions lead to higher production costs. Solution processing is a relatively fast and low-priced technique in fabricating organic films. However, the stacking of several layers on top of each other becomes a great challenge. Fortunately, OLEDs with a mixed single layer structure have attracted wide attention because they hold on a potential for improving the device performance.[7−16] Moreover, it is possible for us to use simple wet-process fabricating means due to its simplest architecture. Baranoff et al. have reported some interesting differences in phosphorescent OLEDs when prepared using solution based or vacuum based techniques.[17] Because the solution- and vacuum-processed depositing routes require organic materials with very different physical properties, in particular solubility and thermal stability, respectively, a direct and systematic comparison between OLEDs fabricated by two processing techniques is not easily realized by using a multilayer structure. Whereas, small molecular OLEDs with a mixed single layer structure (MOLOLEDs) make it possible for direct comparison between devices with identical materials and structure but fabricated by the two processing methods. It will be interesting and valuable information can be achieved if a direct comparison between devices fabricated by vac and sol processing was realized.

Recently, we have investigated 5,6,11,12-tetraphenylnaphthacene (rubrene) based small molecular MOLOLEDs by

Received: March 24, 2011
Accepted: June 13, 2011
Published: June 13, 2011

dx.doi.org/10.1021/am2003729 | ACS Appl. Mater. Interfaces 2011, 3, 2496–2503

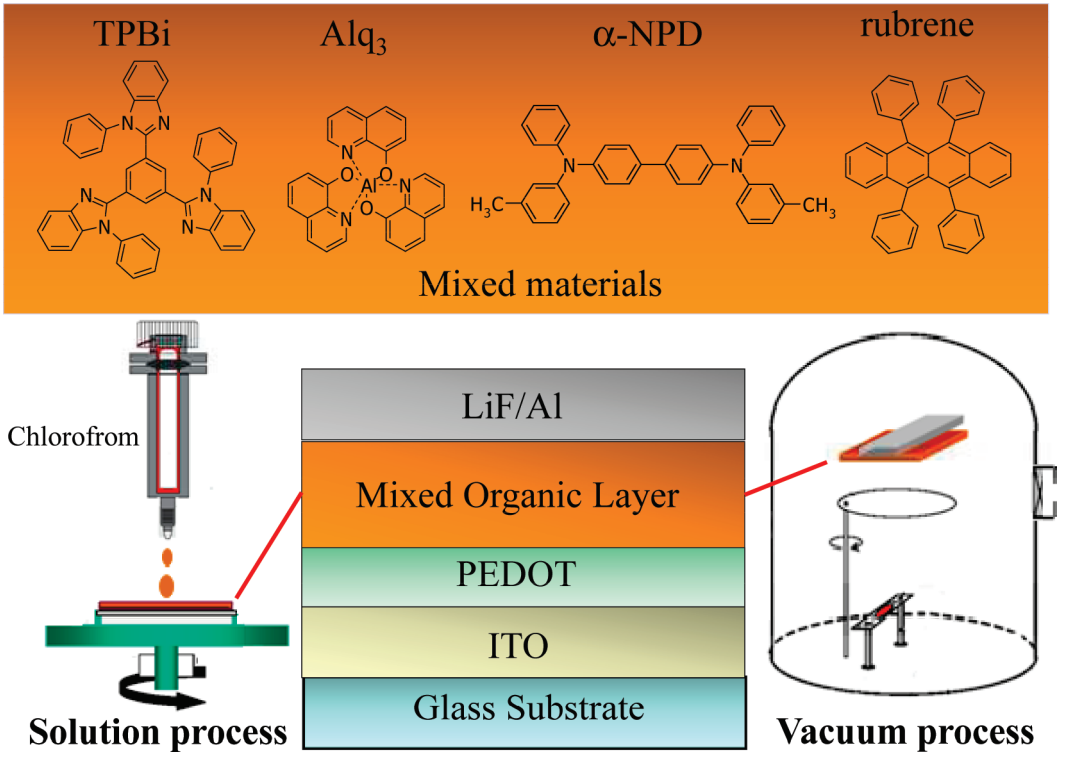

Figure 1. Structures of organic materials upon investigation and a schematic illustration of device structure of MOLOLEDs fabricated by solution- and vacuum-processed methods.

vac processing method. Almost identical device performance is achieved compared with stacked heterostructure device.[18−20] And the roll-off in device efficiency is largely improved after codoping suitable dyes in mixed organic layer.[20] By using suitable solvent, the small molecular MOLOLEDs is expected to be realized using sol processing. In this study, we compare the two processing methods for fabricating MOLOLEDs using rubrene dye as a dopant, in combination with those represented materials usually used in multilayer devices. A Schematic illustration of the materials and structure of MOLOLEDs fabricated by sol and vac processing is shown in Figure 1. In addition, the morphology of mixed organic layer and interfacial conditions between the electrodes and mixed organic layer are of paramount importance for the device performance. For a sol processing device, the presence of a thin insulating layer is probable due to a wet process included in the device fabrication.[21] The crystallization in mixed organic film is also different from that in pure organic layer.[22] It also can be expected that the morphology of mixed organic films and interfacial conditions between the electrodes and mixed organic layer obtained by the two processing methods are quite different. All of these will be expected to affect the carrier injection and transport in MOLOLEDs and further impact on device performance. A direct and systematic comparison of charge injection and transport between devices fabricated by two processing techniques is also shown in this article.

2. EXPERIMENTAL SECTION

In emission device fabrication, indium-tin-oxide (ITO) is used as the anode. Patterned ITO substrate is thoroughly cleaned and ultraviolet (UV) light is irradiated in a UV ozone chamber under O_2 ambient. Then, poly (3,4-ethylenedioxythiophene) (PEDOT) is spin-coated (500 rpm for 5 s and 2500 rpm for 60 s) on ITO following an annealing process at 200 °C for 5 min in the air. Mixed organic layer (MOL) is consisted of electron injection material 1,3,5-tris[2-N-phenylbenzimidazolyl)benzene (TPBi), electron transport material tris-(8-hydroxy-quinoline) aluminum (Alq_3), hole transport material 4,4′-bis[N-(1-napthyl)-N-phenyl-amino] biphenyl (α-NPD) and dopant 5,6,11,12-tetraphenylnaphthacene (rubrene) with some mixing ratio in weight. MOL is spin-coated (2,500 rpm for 60 s) using 1.0 wt % solution for solution-processed device. Two different solvents, chloroform and toluene, are used for comparison. The spin-coated substrate is immediately moved to a vacuum deposition chamber, and baking is carried out with 1 h under 60 °C for chloroform solvent and 110 °C for toluene solvent. When fabricating MOL for vacuum-processed device, the four organic materials are mixed with a desired ratio first. Then, placing mixed organic materials into only one source boat, the mixed layer is deposited with a high deposition ratio of 3−5 Å/s ensuring all organic materials being evaporated. Finally, LiF and Al are evaporated at a base pressure of about 4×10^{-6} Torr. Mixed single layer OLEDs have a structure of ITO/PEDOT (50 nm)/α-NPD + Alq_3 + TPBi + rubrene (110 nm)/LiF (1 nm)/Al (70 nm). For comparison, a multilayer OLED with a structure of ITO/PEDOT (50 nm)/ α-NPD (40 nm)/Alq_3+rubrene [20:1] (50 nm)/TPBi (20 nm)/LiF (1 nm)/Al (70 nm) is also fabricated. The device area is 2×2 mm^2. Devices are encapsulated using counter glass substrate filled with molecular sieve in a dry nitrogen glovebox. Device characteristics are measured using semiconductor parameter analyzer (HP 4155B) and luminance meter (Topcon BM-3). Surface morphology of the mixed organic films is evaluated using an atomic force microscope (AFM; Digital Instrument Nanoscope III).

Hole-dominated device (HDD) with a structure of Au (30 nm)/MoO_3 (20 nm)/MOL (110 nm)/MoO_3 (20 nm)/Au (30 nm) and electron-dominated device (EDD) with a structure of Al (30 nm)/MOL (110 nm)/Al (30 nm) are fabricated using the solution and vacuum-processed means, respectively, for evaluating the temperature dependence of current density and voltage ($J-V$) characteristics at temperature range 173−293 K.

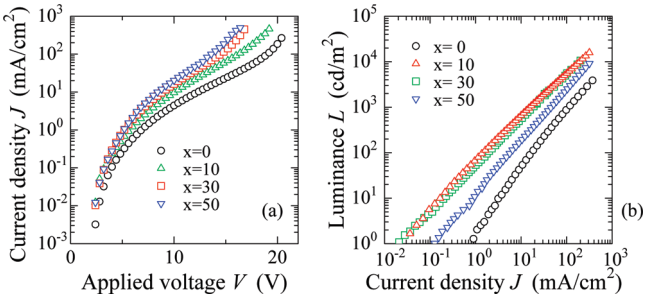

Figure 2. (a) Current density vs voltage ($J-V$) and (b) Luminance vs current density (L−J) characteristics of solution-processed MOLOLEDs with varied mixing ratio of α-NPD x. For all devices, α-NPD:Alq_3:TPBi:rubrene = x:(100 − x)/2:(100 − x)/2:1 in weight.

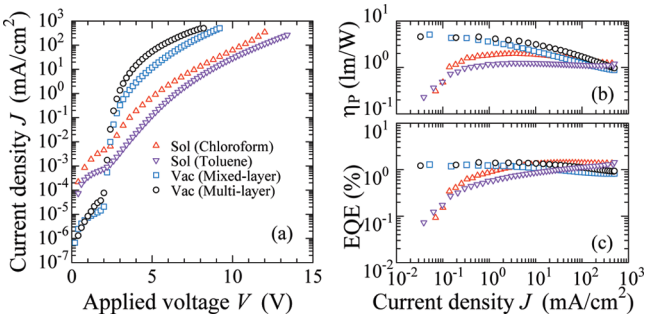

Figure 3. (a) Current density vs voltage ($J-V$), (b) power efficiency η_P, and (c) external quantum efficiency (EQE) characteristics of devices fabricated by vac and sol processing. In mixed organic layer, TPBi: Alq_3: α-NPD: rubrene = 45:45:10:1 in weight.

3. RESULTS

3.1. Comparison of Device Characteristics. In a first study, we investigated the dependence of mixing ratio in organic materials on the device performance. It is found that the device performance is strongly dependent on the mixing ratio of organic material in mixed organic layer. Here, we carry it out by varying the ratio of hole transport material α-NPD in mixed organic layer. Panels a and b in Figure 2 shows the electroluminescence (EL) performance of solution-processed MOLOLEDs (chloroform used as solvent) with various α-NPD ratio x. A decreasing of driving voltage at 100 mA/cm^2 from 19.0 to 13.6 V is observed with increasing of α-the α-NPD ratio from 0 to 50. The driving voltage in mixed organic layer devices is slightly higher than that in heterostructure devices, which is related to the larger hopping distance of hole transport in mixed single layer with respect to heterostructure devices.[23,24] Meanwhile, the luminescence characteristics are also strongly dependent on the mixing ratio of organic materials in mixed organic layer. A maximum luminance of 16 000 cd/m^2 is achieved at 320 mA/cm^2 when x = 10. The balance between the numbers of electrons and holes in the emissive layer is of importance for the EL performance. In general, holes always show higher carrier mobility than electrons in organic materials.[25,26] In the present case, a small quantity of α-NPD (x = 10) is suitable to match other organic materials and achieve relative balance of holes and electrons in mixed organic layer, resulting in good EL performance.

The morphology of the organic layer is of paramount importance for the device performance, and it will be expected that the film morphology on the nanoscopic scale obtained by the two processing will be quite different. For vacuum-deposited organic films, the important parameters are the deposition rate and the substrate temperature. It has been acceptable that the perfect organic films can be achieved by controlling the deposition rate at 1−3 Å/s at room temperature. Whereas for solution-processed organic films because of the wet process, the film morphology are strongly affected by the relative solubility of the organic materials, the solvent, and baking conditions. The AFM observation of the surface morphology of mixed organic films with varied α-NPD ratio is also carried out. For film with x = 0, many raised portions with a maximum height of 20 nm are observed. It is supposed that these raised portions were originated from the crystallization of Alq_3 due to its instability. The surface morphology becomes gradually smooth with increasing of α-NPD and the raised portions disappear when x = 50, which is easily understood because the crystallization of mixed organic molecules can be suppressed and the stability can be improved in contrast with pure organic material.[22] Although surface morphology of mixed organic films is also strongly dependent on the mixing ratio of Alq_3, the balance of holes and electrons plays a more important role on the device performance. There exists a trade-off between carrier balance and surface morphology in mixed organic films. In the case of x = 10, we suppose that the surface morphology of mixed organic films was not largely deteriorated, and a better balance for holes and electrons was achieved.

Figure 3 shows the current density vs voltage ($J-V$), power efficiency η_P and external quantum efficiency (EQE) characteristics of multilayer and mixed organic layer devices fabricated by vac and sol processing, respectively. Among four devices, the vacuum-evaporated device with a multilayer structure exhibits the best device performance. While, there exists no large difference for device performance between other three mixed layer devices and multilayer device at high current densites. Some properties of solvent such as boiling point temperature (T_b) also affect the film formation in solution-processed devices. In present case, Chloroform (T_b: 61.2 °C) and Toluene (T_b: 110.6 °C) are selected as solvents for comparison. It is seen that the device with Chloroform acting as solvent exhibits a relative better device performance with a good EL emission image. In general, small molecular organic material has a low glass-transition temperature (T_g). When using toluene as solvent, the baking has to be done under high-temperature for removing solvent in organic films, which deteriorates the crystallization of organic materials and result in poor device performance. This is also reflected in the EL emission images.

In addition, it is obvious that leakage current in solution-processed devices is larger than that in vacuum-evaporated devices. We ascribe it to a wet process being included in fabrication of a solution-processed device. With a wet process, solvent may remain in the organic films. The film morphology, playing an important role on the formation of metal/organic interfaces, is affected largely by remained solvent or by baking process. On the other hand, it is noticeable that the efficiency characteristics are different between devices by two different processing methods. At lower current densities, the power efficiency and external quantum efficiency of sol-processing devices are lower than that of vac-processing devices, which are related to the large leakage current in sol-processing devices as observed in $J-V$ characteristics. However, at higher current densities, the power efficiency and external quantum efficiency of sol-processing devices are

higher than that of vac-processing devices. As different melting temperature of four organic materials and instable evaporating rate, it is difficult for vac-processing to ensure the formation of uniform distribution for all organic materials in mixed organic layer. Conversely, the sol processing can do it easily because of its wet-processing merit. Of course, the uniform distribution of organic materials in solution-processing devices also has an effect at low current densities. The leak current is large in solution-processing devices, and it dominates the main current in low current densities, which results in lower device efficiency compared with vacuum-processed devices. With increasing current density, the effect of uniform material distribution is preferred to that of leak current, which results in higher device efficiency in high current densities. It suggests that a solution-processed device is excellent for uniform material distribution in mixed organic single layer.

3.2. Comparison of Conduction Mechanism. Two competing electronic processes, namely carrier injection from the contacts and charge conduction in the organic bulk, should be taken into account when analyzing the charge transport measurements because of their importance for understanding the operations of all organic electronics. Much work has been carried out about the carrier injection at organic/metal interface and charge transport in past years.[27−35] Therein, Parker studied the carrier injection process in polymer light emitting devices (PLEDs) and assigned the currents to tunneling mechanism.[27] Campbell et al. found that the current−voltage characteristics in PLEDs can be well fitted by trap-controlled space charge limited current theory.[28] Matsumura et al. ascribed the electron injection from a magnesium cathode to organic layer represented by Alq_3 to thermionic emission mechanism.[29] And a transition from injection-limited to space-limited carrier behavior was experimentally observed in Ag-Pentacene liked diodes from the studies of Zheng et al.[30] In spite of significant advances in the understanding of the qualitative behavior of OLEDs, a fully quantitative description of charge injection at the electrodes, charge transport in the active layer has not yet to be done due to poor understanding of organic/metal interfaces compared with metal/inorganic interfaces. Particularly, the studies about charge transport in solution-processed small molecular mixed single layer OLEDs cannot be found in the literature. Here, we investigate the single-carrier behavior in small molecular MOLOLEDs and compare their difference between devices fabricated by sol and vac processing in detail. It will be expected to provide useful information for understanding the interfacial properties in devices fabricated by two different fabricating means.

3.2.1. Hole-Dominated Devices. The temperature dependent current density−voltage ($J-V$) characteristics in the hole dominated devices is shown in Figure 4a, b for sol processing device and vac processing device, respectively. For solution-processed device, two distinct regions are seen in a log−log representation. In the low bias region, the slope is about 2 and temperature dependence of current density is obvious. The slope in the high bias region shows a large change with temperature from 7.4 to 8.8 upon cooling from 273 to 233 K. For vacuum-evaporated device, J increases smoothly with V under whole voltage range and obvious temperature dependence of $J-V$ characteristics is observed.

First, the $J-V$ characteristics in the solution-processed device are analyzed. In the low bias region (corresponding to an electric field <9 × 10^5 V cm^{-1}), the temperature-dependent $J-V$ curves can be well fitted by Schottky thermal

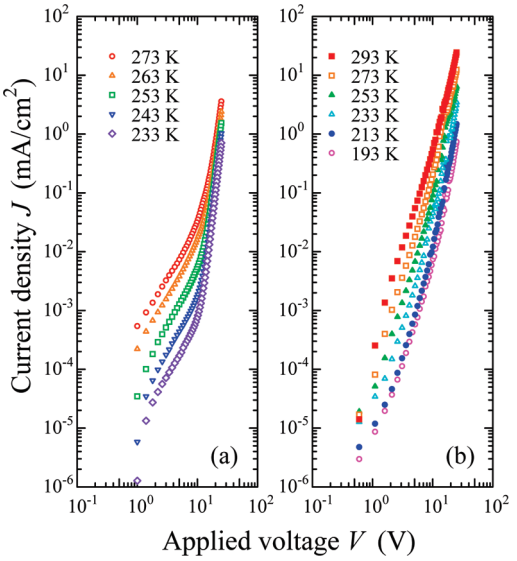

Figure 4. Temperature-dependent $J-V$ characteristics of (a) solution-processed and (b) vacuum-processed HDDs with a structure Au/MoO_3 /MOL/MoO_3 /Au.

emission mechanism as following[36]

$$J = A^{*}T^{2}exp\left[\frac{-q\left(\varphi_{B}-\sqrt{\frac{qV}{4\pi\varepsilon_{i}d}}\right)}{kT}\right] \quad (1)$$

where A^* is the effective Richardson constant, T the temperature, φ_B the barrier height at the interface, q the electronic charge, V the applied voltage, ε_i the dielectric permittivity of the mixed organic layer, d the thickness of mixed single organic layer, and k the Boltzmann constant. In Figure 5 (a), the $J-V$ characteristics are plotted with the relationship ln J vs $V^{1/2}$. By extrapolating straight lines to the ordinal point, the current densities at zero voltage J_0 under different temperature are determined. Using determined J_0 values, the relationship between ln J_0/T^2 vs $1/T$ is plotted, as shown in the inset of Figure 5 (a). The slope of the extrapolated line gives a barrier height of 0.48 eV for hole injection from Au/MoO_3 into mixed organic layer.

The $J-V$ characteristics in high applied bias (corresponding to electric field >9 × 10^5 V cm^{-1}) is analyzed in terms of a power law

$$J = KV^{m} \quad (2)$$

where K is a constant, m (= $E_t/kT+1$) the power law exponent, and E_t the characteristics energy. By fitting the temperature dependence of the exponent m, a characteristics energy E_t = 0.18 eV is extracted. It suggests that hole transport was bulk trapped in high bias. The bulk trap density can be estimated by a differential method,[37] which is usually used in amorphous silicon semiconductor for evaluating the bulk trap density. The bulk trap density is about 10^{18} cm^{-3} under different temperature.[38] In the present device, rubrene liked materials are mixed in the single organic layer, which is assumed to be the main reason for the trap generation. There exists a not large change for bulk trap density

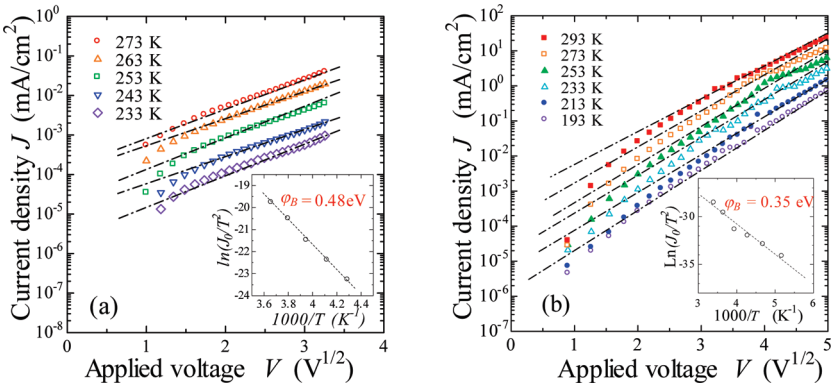

Figure 5. (a) Relationship between ln J and $V^{1/2}$ at low bias (<10 V) for solution-processed HDD with a structure Au/MoO_3/ MOL/MoO_3/Au device; (b) relationship between ln J and $V^{1/2}$ at low bias (<10 V) for vacuum-processed HDD with a structure Au/MoO_3/MOL/MoO_3/Au device. Inset are the relationships between ln J_0/T^2 and $1/T$. J_0 are obtained by extrapolating in $V = 0$.

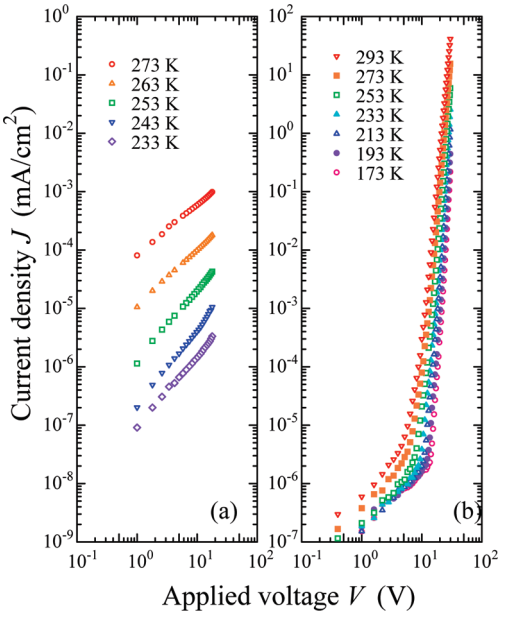

Figure 6. Temperature-dependent $J-V$ characteristics of (a) solution-processed and (b) vacuum-processed electron-dominated devices with a structure Al//MOL/Al.

in the temperature range 273−233 K due to carrier freezing in this lower temperature range.

For vacuum-evaporated device, the fitting using the tunneling or space charge limited current (SCLC) models are not well agreed with experimental $J-V$ curves. The obvious temperature dependence of $J-V$ characteristics implies that hole injection from the anode to mixed organic layer in a vacuum-evaporated device could be ascribed to Schottky thermal emission at whole measured voltage. With same fitting in the solution-processed device, the barrier height in a vacuum-evaporated device is determined to be 0.35 eV. The typical evaluated results are shown in Figure 5b and inset.

3.2.2. Electron-Dominated Devices. The temperature dependent $J-V$ characteristics in electron dominated devices is shown in panels a and b Figure 6 for sol and vac device, respectively. For solution-processed device, J increases smoothly with V in whole voltage range and obvious temperature dependence of $J-V$ characteristics is observed. For vacuum-evaporated device, two distinct regions are seen in the $J-V$ curves in a log−log representation. The slope in the low bias region is about 1 and temperature dependence of J is obvious. In the high bias region, J increases rapidly with V and the temperature dependence is also observed.

In the solution-processed device, the current density is smaller than that in a corresponding hole dominated device under same temperature due to electrons always showing lower mobility than holes. By fitting based on Schottky thermal emission, the barrier height at Al/MOL interface in a solution-processed device is determined to be 0.84 eV. The typical evaluated results are shown in Figure 7a and inset.

For vacuum-evaporated device, the $J-V$ characteristics at the lower bias region are analyzed first. In a log−log representation, J is proportional to V in this region. The relationship between conductivity and temperature based on a hopping model is expressed as[39]

$$\sigma \propto exp[ST^{-1/(n+1)}] \qquad (3)$$

where σ is the conductivity, S a constant, T the temperature and n the dimension (0, 1, 2 or 3). The calculated conductivities are in good agreement with eq 3 when $n = 3$. It demonstrates that the conduction mechanism of electron in vacuum-evaporated electron-dominated devices at lower voltage is ascribed to be three-dimensional variable-range hopping (VRH) model.

With increasing of applied voltage, J increases rapidly with V and the temperature dependence of $J-V$ characteristics is obvious in the higher bias region. A barrier height of 0.76 eV at Al/MOL interface in a vacuum-evaporated device is achieved by fitting based on Schottky thermal emission mechanism. The typical evaluated results are shown in Figure 7b and inset.

4. DISCUSSION

The above results demonstrate that the charge injection and conduction mechanism is very different between solution- and vacuum-evaporated devices using same materials and structure. For better understanding, energy levels of organic materials and work functions upon investigation are shown in Figure 8. Obviously, the barrier height is not equal to the difference between the work functions of electrodes and energy level of organic materials regardless in solution- or vacuum-evaporated devices. It

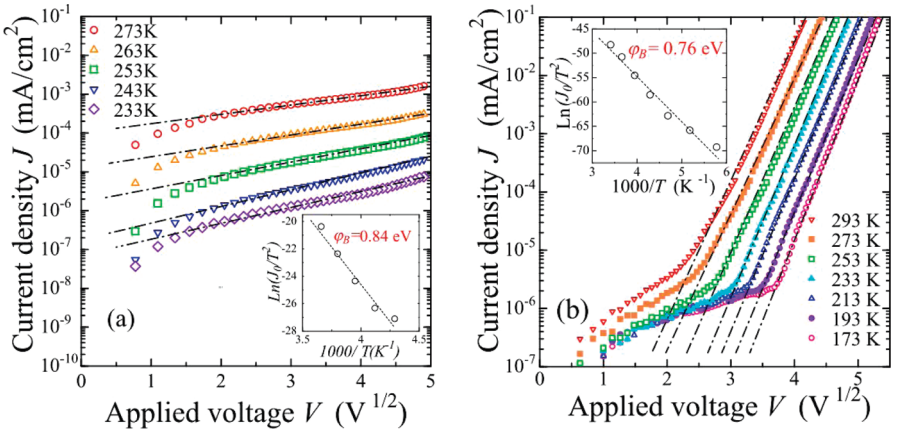

Figure 7. (a) Relationship between ln J and $V^{1/2}$ for solution-processed Al/MOL/Al device; (b) relationship between ln J and $V^{1/2}$ at high bias (>10 V) for vacuum-processed EDD with a structure Al//MOL/Al device. Inset are the relationships between ln J_0/T^2 and $1/T$. J_0 are obtained by extrapolating in $V = 0$.

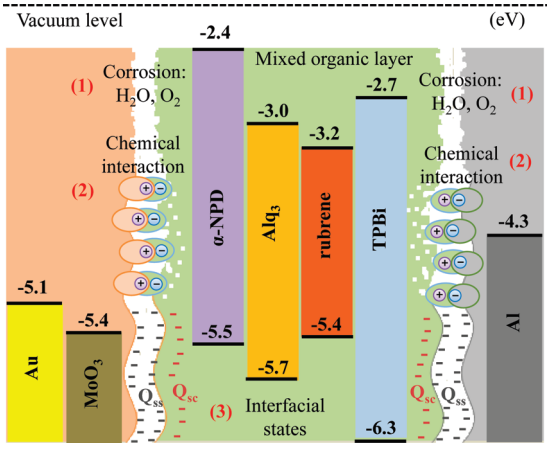

Figure 8. Energy levels of organic materials and work functions of metals upon investigations in combination with a schematic illustration of the possible factors forming and affecting the interfaces in solution- and vacuum-processed devices.

implies that some changes occurred at the interfaces of metals/MOL in these devices. The key role of the interface at organic/metal is well acknowledged in the context of organic optoelectronic devices and the formation of a thin interfacial layer between a metal and organic layer has been confirmed experimentally.[40−44] Particularly, Ishii et al. investigated and summarized the progress in the understanding of the interfacial electronic structures at organic/metal and organic/organic interfaces.[40] They pointed out the key factors affecting interfacial electronic structures at organic/metal interfaces as following: (1) effect of the device fabricating circumstance; (2) other types of chemical interaction than charge transfer between the organic and metal layers; (3) the possible existence of interfacial state. (4) electron transfer between the metal and the organic layer with the positive and negative charges separated across the interface; (5) the image effect or the modification of the surface dipole at the metal surface; (6) orientation of polar molecules or functional groups.

Combined with present devices, we suppose that circumstance effect, chemical interaction and interfacial state were the main factors for the large difference between *sol*- and *vac*-processed devices. A schematic illustration of the possible factors for forming and affecting the interfaces is also shown in Figure 8. First, the electronic properties of organic devices are significantly affected by the device fabricating circumstance. When the device is exposed to air or place in the low vacuum, the metal surface is usually oxidized and the absorption of molecules like oxygen and water may also remain in organic films,[40] which usually results in asymmetry forward and backward $J-V$ characteristics for the metal/organic/metal device with a sandwich structure.[42] In the case of a wet process, such as spin-coating, solvents may remain in the organic film even if a baking is carried out. The actual devices are usually fabricated under such conditions, and significant effects of fabricating circumstance on various electric properties are known. In our present devices, the symmetric forward and backward $J-V$ characteristics are both observed in sol- and vac-processed symmetric sandwich devices. It is implied that not the metal oxidization due to poor vacuum, but remained solvent in mixed organic layer due to inadequate baking was one of the main factors for the large difference of charge conduction between sol- and vac-processed devices.

When metal is deposited on an organic layer by evaporation, the high reactivity of the vaporized metal atom often leads to a chemical reaction at organic/metal interface.[40] It is also known that metal atoms may diffuse into the organic layer.[45−47] These chemical reactions will depend sensitively on the morphology and chemistry conditions at organic/metal interface. In contrast, the chemical interaction situation in a vacuum process is usually milder than that in a solution process. Figure 9 shows the AFM observation of surface morphology for *sol*- and *vac*-processed small molecular mixed organic films. Obviously, a porous surface morphology appeared in sol-processed films in contrast with vac-processed films due to a baking included in sol-processed devices. It is supposed that the chemical reaction such as the diffusing of metal atoms occurred easily in solution-processed devices. Therefore, we assume that the chemical interaction at MOL/metal MOL/metal interface also played an important role on the charge conduction mechanism in our devices.

As mentioned above, the barrier height is not equal to the difference between the work functions of electrodes and energy level of organic materials in present devices. Actually, barrier height at an organic/metal interface depends not only on the work function of metals, but also on the interfacial conditions, such as the interfacial state which affects the charge exchange

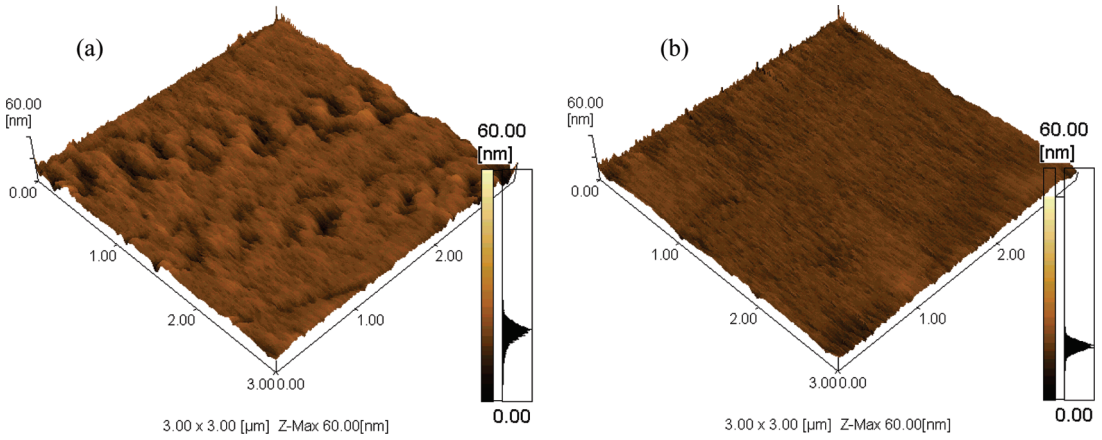

Figure 9. AFM surface morphology of mixed organic films fabricated by (a) solution process and (b) vacuum process.

between the metal and the organic layer. Such interfacial state is well-known in inorganic semiconductor, and ascribed to various intrinsic and extrinsic origins such as metal-induced gap states (MIGS) formed by the penetration of metal wave functions into semiconductor.[48−50] In the case of organic semiconductor, the surface state charge (Q_{ss}) at interface and space charge (Q_{sc}) in organic layer is created due to the changes of roughness in molecule order and electronic states when an organic layer is contracted with a metal. The interfacial conditions will be determined by the redistribution of these generated charges. Although the origin in the case of organic/metal contact may be different from inorganic/metal contact, there seems to be some analogous mechanisms (interfacial state) to affect the charge conduction in most of these systems.

5. CONCLUSIONS

As a summary, we have presented the first comparison of MOLOLEDs in which the mixed organic layer is fabricated by the two commonly used deposition techniques, spin-coating for solution (sol) and vacuum deposition (vac). An almost same luminescence characteristic is achieved in two devices fabricated by different processing methods. The performance of a solution-processed device is strongly dependent on the mixing ratio of organic materials and the surface morphology of mixed organic films. Meanwhile, a solution-processed device is found to be excellent for the formation of a uniform material distribution in mixed organic layer. From the evaluation of temperature dependence in the hole and electron-dominated devices fabricated by two processing methods, the charge injection and conduction mechanism is found to be very different in two different processed devices. It is supposed that circumstance effect, chemical interaction and interfacial states were the main factors for the large difference of charge conduction.

Overall, in our class of materials, solution processing leads to an almost identical luminescence characteristic with vacuum processing. Because of the merit of wet-processing, solution processing make it easy to realize a uniform distribution of materials in mixed organic films, which is beneficial for luminescence performance at the high current density. Solution processing shows clear advantages on fabricating OLEDs such as its high processing speed and capabilities of the low-cost and large area. On the other hand, carrier conduction plays an important role on the operation of organic electronic devices. Interfaces between organic and metal have been identified as being of particular importance for device function and efficiency. Despite the larger number of published literatures including our investigations in this work, there is still a lack of a truly comprehensive picture of the mechanism that determines the properties of such interfaces, and how these interfaces can predictably be designed and fabricated to satisfy certain requirements. This will require extensive concerted experimental and theoretical efforts to clearly expound the detailed mechanisms. More importantly, the finding in this article stimulates the implementation of advanced spectroscopy diagnostics such as ultraviolet photoelectron spectroscopy for the investigation of charge transfer and their dynamics at organic/metal interfaces in organic electronic devices that are fabricated using the solution- and vacuum-processed methods.

■ ASSOCIATED CONTENT

Supporting Information. AFM surface morphology of solution-processed mixed film, EL emission images of solution- and vacuum-processed devices, variation of the exponent m with T in solution-processed HDD (>10 V), and temperature dependence of conductivity in vacuum-processed EDD (<10 V). This material is available free of charge via the Internet at http://pubs.acs.org.

■ AUTHOR INFORMATION

Corresponding Author

*E-mail: zhaokuiwang@hotmail.com. Tel: +81-76-445-6731. Fax: +81-76-445-6732.

■ ACKNOWLEDGMENT

This work is partly supported by regional innovation of R&D projects, overseen by the Ministry of Economy, Trade and Industry (METI), Japan.

■ REFERENCES

(1) Tang, C. W.; VanSlyke, S. A. *Appl. Phys. Lett.* **1987**, *51*, 913.
(2) Tang, C. W.; VanSlyke, S. A.; Chen, C. H. *J. Appl. Phys.* **1989**, *65*, 3610.
(3) Ma, D.; Hümmelgen, I. A.; Jing, X.; Hong, Z.; Wang, L.; Zhao, X.; Wang, F.; Karasz, F. *J. Appl. Phys.* **2000**, *87*, 312.

(4) Ma, D.; Hümmelgen, I. A.; Jing, X.; Wang, D.; Hong, Z.; Wang, L.; Zhao, X.; Wang, F. *Braz. J. Phys.* **2000**, *30*, 392.
(5) Chwang, A. B.; Kwong, R. C.; Brown, J. J. *Appl. Phys. Lett.* **2001**, *80*, 725.
(6) Adachi, C.; Tsutsui, T.; Saito, S. *Appl. Phys. Lett.* **1989**, *55*, 1489.
(7) Greenham, N. C.; Moratti, S. C.; Bradley, D. D. C.; Friend, R. H.; Holmes, A. B. *Nature London* **1993**, *365*, 628.
(8) Naka, S.; Shinno, K.; Okada, H.; Onnagawa, H.; Miyashita, K. *Jpn. J. Appl. Phys.* **1994**, *33*, L1772.
(9) Vissengerg, M. C. J. M.; Jong, M. J. M. *Phys. Rev. B* **1998**, *57*, 2667.
(10) Cao, Y.; Parker, I. D.; Zhang, C.; Heeger, A. J. *Nature London* **1999**, *397*, 414.
(11) Jing, Y. D.; Yang, J. P.; Heremans, P. L.; Auweraer, M. V.; Rousseau, E.; Geise, N. J.; Borghs, G. *Chem. Phys. Lett.* **2000**, *320*, 387.
(12) Matsumura, M.; Manabe, K. *Appl. Phys. Lett.* **2001**, *79*, 4491.
(13) Aziz, H.; Popovic, Z. D.; Hu, N.-X.; Hor, A. M.; Xu, G. *Science* **1999**, *283*, 1900.
(14) Pfeiffer, M.; Forrest, S. R.; Leo, K.; Thompson, M. E. *Adv. Mater.* **2002**, *14*, 1633.
(15) Rost, C.; Karg, S.; Riess, W.; Loi, M. A.; Murgia, M.; Muccini, M. *Appl. Phys. Lett.* **2004**, *85*, 1613.
(16) Aziz, H.; Popovic, Z. D.; Hu, N. -X. *Appl. Phys. Lett.* **2002**, *81*, 370.
(17) Baranoff, E.; Bolink, H. J.; Angelis, F. D.; Fantacci, S.; Censo, D. D.; Djellab, K.; Grätzel, M.; Nazeeruddin, M. K. *Dalton Trans.* **2010**, *39*, 8914.
(18) Wang, Z. K.; Naka, S.; Okada, H. *Appl. Phys. A: Mater. Sci. Process.* **2010**, *100*, 1103.
(19) Wang, Z. K.; Lou, Y. H.; Naka, S.; Okada, H. *J. Lumin.* **2010**, *130*, 1198.
(20) Wang, Z. K.; Lou, Y. H.; Naka, S.; Okada, H. *Appl. Phys. Lett.* **2010**, *97*, 203302.
(21) Dannetun, P.; Fahlman, M.; Fauquek, C.; kaerijama, K.; Sonoda, Y.; Lazzaroni, R.; Brédas, J. L.; Salaneck, W. R. *Synth. Met.* **1994**, *67*, 133.
(22) Markham, J. P. J.; Lo, S.-C.; Magennis, S. W.; Burn, P. L.; Samuel, I. D. W. *Appl. Phys. Lett.* **2002**, *80*, 2645.
(23) Uchida, M.; Adachi, C.; Koyama, T.; Taniguchi, Y. *J. Appl. Phys.* **2000**, *86*, 1680.
(24) Ma, D.; Lee, C. S.; Lee, S. T.; Hung, L. S. *Appl. Phys. Lett.* **2002**, *80*, 3641.
(25) Martens, H. C. F.; Huiberts, J. N.; Blom, P. W. M. *Appl. Phys. Lett.* **2000**, *77*, 1852.
(26) Matine, D. L.; Woo, H. S.; He, W.; Kim, T. W.; Kippelen, B.; Peyghambarian, N. *Appl. Phys. Lett.* **2000**, *76*, 3849.
(27) Parker, I. D. *J. Appl. Phys.* **1994**, *75*, 1658.
(28) Campbell, A. J.; Weaver, M. S.; Lidzey, D. G.; Bradley, D. D. C. *J. Appl. Phys.* **1998**, *84*, 6737.
(29) Matsumura, M.; Akai, T.; Satito, M.; Kimura, T. *J. Appl. Phys.* **1996**, *79*, 264.
(30) Zheng, Y.; Wee, A. T. S.; Troadec, C.; Chandrasekhar, N. *Appl. Phys. Lett.* **2009**, *95*, 143303.
(31) Abkowitz, M. A.; Mizes, H. A.; Facci, J. S. *Appl. Phys. Lett.* **1995**, *66*, 1288.
(32) Worne, J. H.; Anthony, J. E.; natelson, D. *Appl. Phys. Lett.* **2010**, *96*, 053308.
(33) Scheinert, S.; Paasch, G. *J. Appl. Phys.* **2009**, *105*, 014509.
(34) Ng, T. N.; Silveira, W. R.; Marohn, J. A. *Phys. Rev. Lett.* **2007**, *98*, 066101.
(35) Samanta, S.; Aswal, D. K.; Singh, A.; Debnath, A. K.; Kumar, M. S.; Hayawawa, Y.; Gupta, S. K.; Yakhmi, J. V. *Appl. Phys. Lett.* **2010**, *96*, 013305.
(36) Sze, S. M. *Physics of Semiconductor Device*, 2nd edn, Wiley, New York, 1981, Ch. 5.
(37) Nespurek, S.; Sworakowski, J. *J. Appl. Phys.* **1980**, *51*, 2098.
(38) Wang, Z. K.; Lou, Y. H.; Naka, S.; Okada, H. *Appl. Phys. Lett.* **2011**, *97*, 203302.
(39) Knotch, M. L.; Pollak, M.; Donovan, T. M. *Phys. Rev. Lett.* **1973**, *30*, 853.
(40) Ishi, H.; Sugiyama, K.; Ito, E.; Seki, K. *Adv. Mater.* **1999**, *11*, 605.
(41) Koch, N. *Chem. Phys. Chem.* **2007**, *8*, 1438.
(42) Chen, C.; Hill, I. G.; Kahn, A. *Adv. Mater.* **1999**, *11*, 1523.
(43) Chen, C.; Hill, I. G.; Kahn, A.; Schwartz, J. *J. Am. Chem. Soc.* **2000**, *122*, 5391.
(44) Ma, H.; Yip, H. L.; Huang, F.; Jen, A. K.-Y. *Adv. Funct. Mater.* **2010**, *20*, 1371.
(45) Tarlov, M. J. *Langmuir* **1992**, *8*, 80.
(46) Dannetun, P.; Fahlman, M.; Fauquek, C.; kaerijama, K.; Sonoda, Y.; Lazzaroni, R.; Brédas, J. L.; Salaneck, W. R. *Synth. Met.* **1994**, *67*, 133.
(47) Hirose, Y.; Kahn, A.; Aristov, V.; Soukiassian, P. *J. Appl. Phys.* **1996**, *68*, 217.
(48) Brillson, L. J. *Surf. Sci. Rep* **1982**, *2*, 123.
(49) Monch, W. *Surf. Sci.* **1994**, *299/300*, 909.
(50) Brillson, L. J. *Surf. Sci.* **1994**, *299/300*, 928.